

DISCOVERY OF A MULTIPOLAR STRUCTURE WITH AN EQUATORIAL DISK IN NGC 6072

SUN KWOK¹, SZE-NING CHONG¹, CHIH-HAO HSIA¹, YONG ZHANG¹, AND NICO KONING²

¹ Department of Physics, The University of Hong Kong, Pokfulam Road, Hong Kong, China; sunkwok@hku.hk

² Department of Physics & Astronomy, University of Calgary, Calgary, Alberta T2N 1N4, Canada

Received 2009 June 17; accepted 2009 November 5; published 2009 December 8

ABSTRACT

From near-infrared and molecular hydrogen imaging observations, we have discovered that the planetary nebula NGC 6072 has a multipolar structure with a prominent equatorial ring. We have modeled the object by a double bipolar system, each with an equatorial ring and a pair of bipolar lobes. The bipolar axes of the two systems are estimated to be separated by 47° . The existence of such a double bipolar system suggests that the object has undergone separate fast outflow episodes separated by several thousand years.

Key words: infrared: ISM – planetary nebulae: general – planetary nebulae: individual (NGC 6072)

Online-only material: color figures

1. INTRODUCTION

NGC 6072 (= PNG 342.1+10.8 = My 93 = VV 77 = IRAS 16097–3606) was discovered as a planetary nebula (PN) by Hubble (1921). In the Digital Sky Survey (DSS) optical image, NGC 6072 has the appearance of an elliptical shell in the north–south (N–S) direction with faint extensions in the east–west (E–W) direction (Figure 1). According to Gathier & Pottasch (1988), the central star has a B magnitude of 19.2. Although the nebula has an interesting morphology, it has received very little attention over the years. A search of the NASA ADS results in only six entries with the object included in the paper abstracts, most of them relating to molecular gas in the object. NGC 6072 has strong CO emission, which was detected as early as 1989 (Huggins & Healy 1989). The observed CO line strength in NGC 6072 is among the highest in PN, only weaker than a handful of objects such as NGC 7027 and IRAS 21282+5050. The CO profile in the nebula position is strongly double peaked, indicating the presence of a molecular shell expanding at 15 km s^{-1} . A molecular mass of $0.22 M_\odot$ is estimated from the CO observations (Cox et al. 1991).

In their work of morphological classification of PNs, Corradi & Schwarz (1995) classified NGC 6072 as bipolar, the same classification that they give to NGC 2440, which we now know to be a classic example of multipolar nebula (López et al. 1998). The recent surge of interest in multipolar nebulae (Manchado et al. 1996; Sahai 2000) has prompted us to study the morphology of NGC 6072 in detail, as it shows some signs of multipolar characteristics in its optical image.

In this paper, we use the recently obtained near-infrared images of NGC 6072 to study the morphology of the object, and use a model simulation to determine its three-dimensional structure.

2. OBSERVATIONS AND RESULTS

2.1. *Spitzer* Imaging

The observations were made with the *Spitzer Space Telescope* Infrared Array Camera (IRAC) on 2004 August 12 under program number 68 (PI: Giovanni Fazio). The center position of the images is R.A.(2000) = $16^{\text{h}}12^{\text{m}}58^{\text{s}}20$, decl.(2000) = $-36^\circ 13' 48''.0$. The angular resolution of IRAC is ~ 2 arcsec. The exposure time for each of the bands is 600 s. Figure 2 shows the

IRAC four (3.6, 4.2, 5.8, and $8.0 \mu\text{m}$) band images of NGC 6072 and a color composite of the images is shown in Figure 3.

While a pair of bipolar lobes along the approximate SE–NW direction can be seen in the 3.6 and $4.5 \mu\text{m}$ images (labeled as a and a' in Figure 4), another pair of lobes along the approximate NE–SW (labeled as b and b' in Figure 4) can be seen in the 5.8 and $8.0 \mu\text{m}$ images. Less obvious, but still discernible is a third pair of lobes in the E–W direction (labeled as c and c' in Figure 4). Although the axes of these three pairs of bipolar lobes cannot be precisely defined, they intersect approximately at the position of the central star.

Furthermore, an elliptical ring (or disk) with a major axis along the N–S direction can clearly be seen in all four band images (labeled d in Figure 4). This ring has a major axis of 91 arcsec and a minor axis of 38 arcsec with the major axis at the position angle (P.A.) of 5° . If we assume that this ring is a projection of a circle on the sky, we derive an orientation angle of 25° from the line of sight (0° being viewed edge on).

2.2. *CFHT* Imaging

We have also obtained observations using the Wide-field Infrared Camera (WIRCam) on the Canada–France–Hawaii Telescope (CFHT) under the program 06AT03 on 2006 April 16. WIRCam consists of four HAWAII2-RG detectors each having a 2048×2048 pixel format with a pixel scale of 0.3 arcsec. The total field of view of the camera is $20 \text{ arcmin} \times 20 \text{ arcmin}$. The images of NGC 6853 were taken with a narrow-band molecular hydrogen filter (central wavelength $2.122 \mu\text{m}$, bandwidth $0.032 \mu\text{m}$) and the broadband K_s filter (central wavelength $2.146 \mu\text{m}$, bandwidth $0.325 \mu\text{m}$). Observations of NGC 6072 at the CFHT were made in the nodding mode where a five-position dither pattern is made on target, and then an off-target (sky) frame is taken. The exposure time on each frame for each filter is 30 s and 6 s, respectively. Standard bias subtraction, flat-fielding, and bad pixel masking were performed.

The WIRCAM $\text{H}_2\text{--}K_s$ image of NGC 6072 is shown in Figure 5. The three pairs of lobes in the IRAC image (Figure 4) can also be seen in this image. Again, the equatorial ring is very prominent and has a similar size as estimated from the *Spitzer* image. Also prominent is a horizontal bar located in the N to NW direction. This bar can also be clearly seen in the IRAC images. The sharpness of the bar is highly



Figure 1. Digitized Sky Survey *R*-band image of NGC 6072. North is up and east is to the left.

suggestive of an interaction zone, may be representing a boundary between ionized and neutral matter. We also note that the bar is not straight, but is bent inward near the middle. A less obvious counterpart of this bar may also be present in the S–SE direction. Could these pairs of bars represent the edges of a double cone? The images are not clear enough on this point, but if it is the case, then the axis of the cone would be almost directly on the plane of the sky. If there is indeed such a pair of bars, what is the cause of their wildly different brightness? At first it may seem that the northern bar is closer to us, but in fact the CO map of NGC 6072 shows that the northern part of the nebula is receding and farther away from us whereas the southern part is approaching and nearer to us (Cox et al. 1991).

2.3. *ISO* Spectrum

NGC 6072 was observed by the Short Wavelength Spectrometer (SWS) of *Infrared Space Observatory* (*ISO*) in 1996-09-09 (PI: M. Barlow). The slit position was centered at R.A.(J2000) = $16^{\text{h}}12^{\text{m}}58^{\text{s}}.8$ and decl.(J2000) = $-36^{\circ}13'38''.6$. The on-source integration time of the SWS observation is 1140 s. The apertures of SWS range from $14'' \times 20''$ to $20'' \times 22''$ and therefore should cover most of the nebula.

The Long Wavelength Spectrometer (LWS) observations of this object have been reported by Liu et al. (2001), who performed a line ratio analysis to derive the temperature and density of the nebula. Details of the LWS observations can

Table 1
Fluxes of the Detected Emission Lines in the *ISO* SWS and LWS Spectra

Identification	Wavelength (μm)	Observed Flux ($10^{-10} \text{ erg cm}^{-2} \text{ s}^{-1}$)
SWS:		
[Clv]	11.744	0.08
[Mg v]	13.688	0.04
[Ne iii]	15.557	0.13
[S iii]	18.859	0.10
[O iv]	25.892	0.31
LWS:		
[O iii]	51.809	0.67
[N iii]	57.304	0.28
[O i]	63.177	0.20
[O iii]	88.372	0.50
[N ii]	121.945	0.02
[O i]	145.473	0.01
[C ii]	157.721	0.05

be found there. In Figure 6, we present the combined SWS spectrum of NGC 6072. The measured fluxes of the lines in the spectrum are given in Table 1.

2.4. *Spitzer* Spectroscopy

NGC 6072 was observed with the *Spitzer* Infrared Spectrometer (IRS; Houck et al. 2004) through the observation program 45

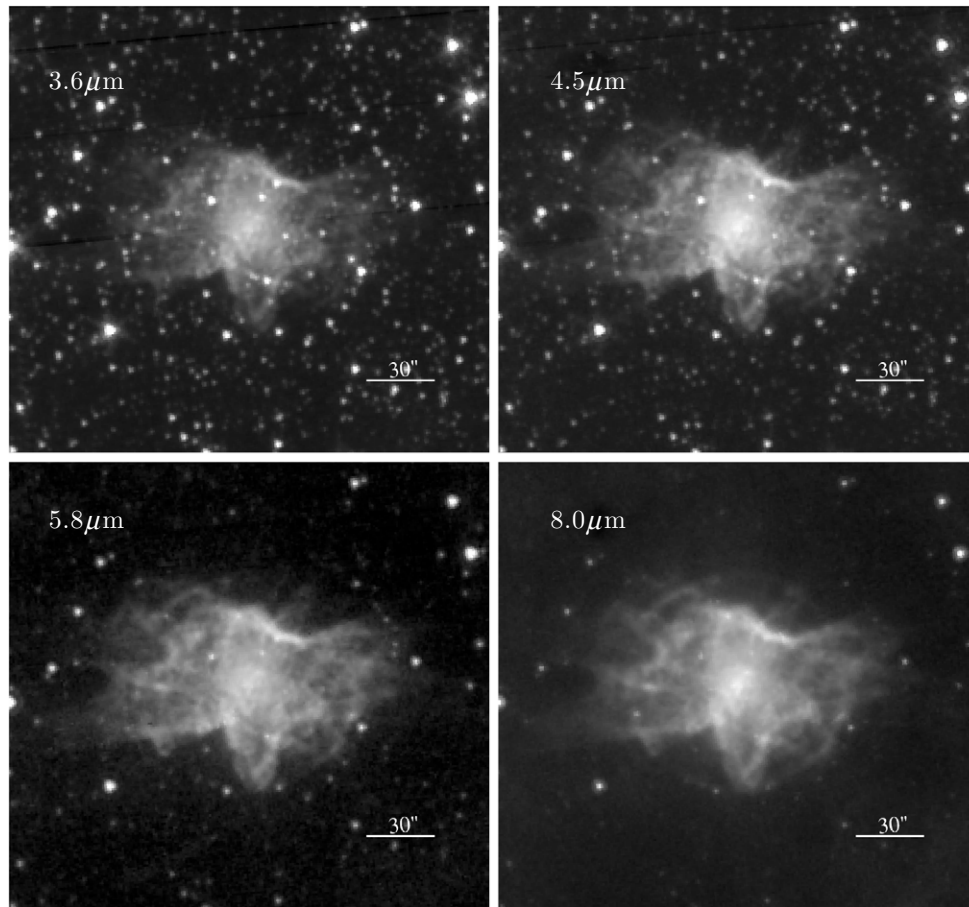


Figure 2. *Spitzer* IRAC images of NGC 6072 at the 3.6, 4.5, 5.8, and 8.0 μm bands. These grayscale images are displayed in log scale to show the fainter outer structures. North is up and east is to the left.



Figure 3. Color composite of the IRAC images of NGC 6072. All four IRAC bands are used in this RGB color composite. The respective weights are Channel 1: $R = 0$, $G = 0$, $B = 132$; Channel 2: $R = 0$, $G = 134$, $B = 0$; Channel 3: $R = 66$, $G = 32$, $B = 0$; Channel 4: $R = 132$, $G = 0$, $B = 0$, where $R = 256$, $G = 256$, $B = 256$ is pure white and 0,0,0 is black.

(A color version of this figure is available in the online journal.)

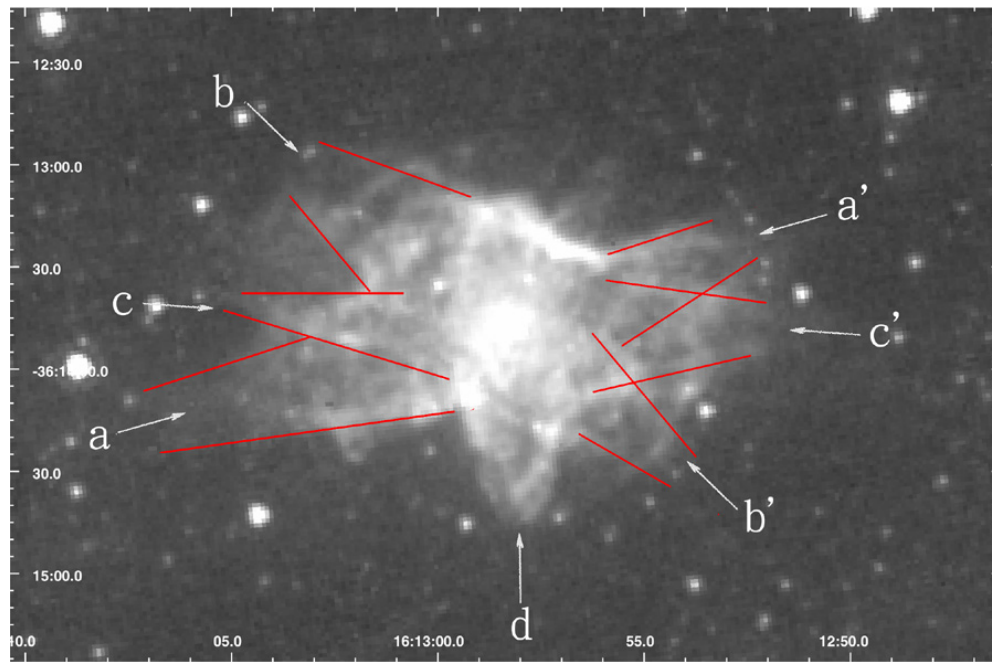


Figure 4. *Spitzer* IRAC 5.8 μm image of NGC 6072 with the three pairs of bipolar lobes marked as $a - a'$, $b - b'$, $c - c'$. The equatorial disk is marked as d . (A color version of this figure is available in the online journal.)

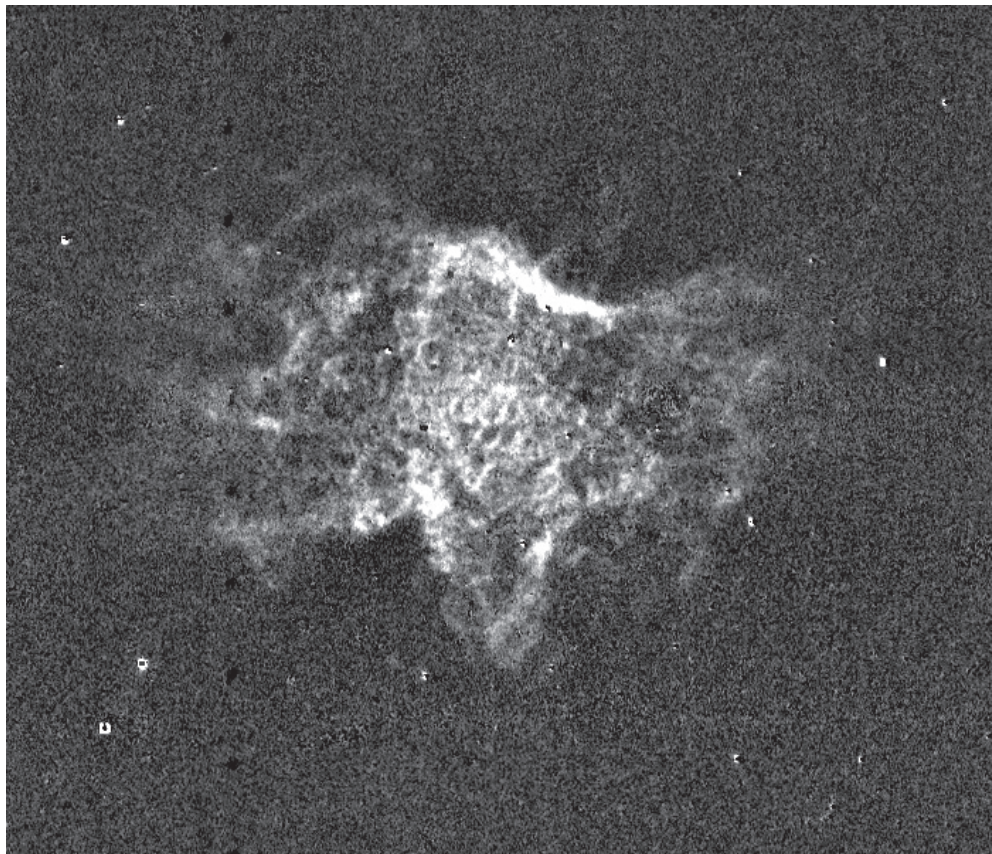


Figure 5. CFHT WIRCam $\text{H}_2\text{-K}_s$ image of NGC 6072. North is up and east is to the left. The size of the image is $3'.5 \times 3'$.

(PI: T. Roellig) with Astronomical Observation Request (AOR) key of 4115200 and 4115456. The spectra were obtained in staring mode using the short high (SH) module (9.9–19.6 μm), and the long high (LH) module (18.7–37.2 μm) with spectral dispersion was of $R \sim 600$, respectively. The position of the IRS slit is positioned at the center of the nebula, with an orientation

of $\text{P.A.} = 272^\circ$. The sizes of the SH and LH slits are $4'.7 \times 11'.3$ and $11'.1 \times 22'.3$, respectively.

Data were reduced starting with basic calibrated data from the *Spitzer* Science Center's pipeline version 17.2 and were processed with the IRSCLEAN program to remove rogue pixels. The SMART analysis package (Higdon et al. 2004) was used

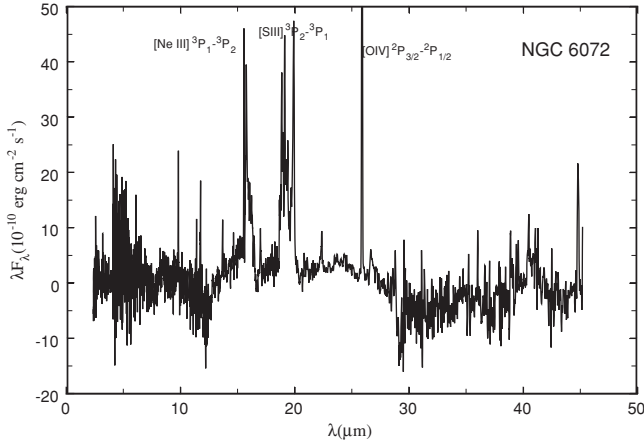
Figure 6. *ISO* SWS spectrum of NGC 6072.

Table 2
Fluxes of the Detected Emission Lines in the *Spitzer* IRS Spectrum

Identification	Wavelength (μm)	Observed Flux ($10^{-10} \text{ erg cm}^{-2} \text{ s}^{-1}$)	Normalized Flux ($10^{-10} \text{ erg cm}^{-2} \text{ s}^{-1}$)
[S IV]	10.51	0.0054	0.034
H I (9–7)	11.31	0.00042	0.003
[Cl IV]	11.76	0.0012	0.008
H I (7–6)	12.37	0.0028	0.018
[Ne II]	12.81	0.011	0.068
[Ar V]	13.09	0.0048	0.030
[Ne V]	14.32	0.017	0.11
[Ne III]	15.55	0.12	0.74
[S III]	18.71	0.0027	0.017
[Ar III]	21.82	0.0010	0.007
[Ne V]	24.32	0.0078	0.049
[O IV]	25.88	0.19	1.18
[S III]	33.47	0.0027	0.017
[Ne III]	36.01	0.0069	0.044

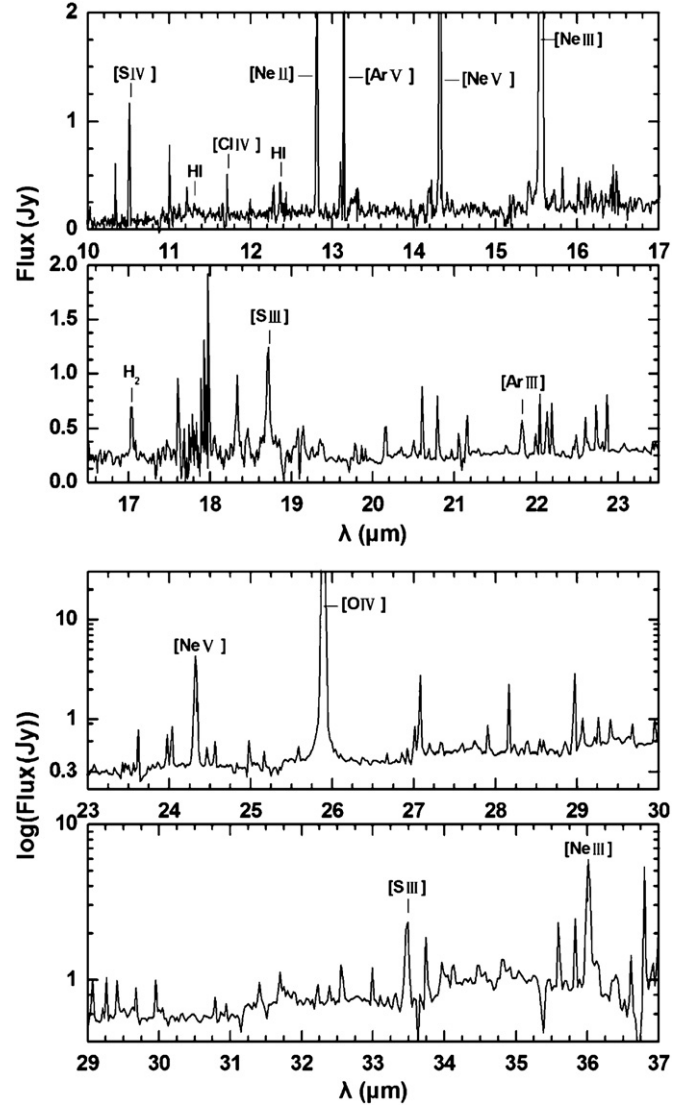
to extract the spectra. The IRS observations were combined to improve the signal-to-noise ratio (S/N), and the resultant spectrum is shown in Figure 7. Since the slit location of the spectrum in the short wavelength range is outside this object, we have plotted only the 10–37 μm part of the spectrum, where the slit lies within the image of the object.

The measured line fluxes in the IRS spectrum are given in Table 2. In Column 3, we attempt to derive the total fluxes over the entire nebula by scaling the observed fluxes by a factor using the theoretical flux ratios between the infrared H I and H β lines. From Case B recombination line theory and an assumed electron temperature of 10,000 K and an electron density of 1000 cm^{-3} , we have H I(9–7)/H β = 0.003 and H I(7–6)/H β = 0.010. These theoretical ratios are then applied to the observed log H β flux of $-11.58 \text{ erg cm}^{-2} \text{ s}^{-1}$ (Acker et al. 1992) to derive the scaling factor of 6.4 for the IRS spectrum.

We note that there are some differences between *ISO* and IRS spectra which cannot be explained entirely by the difference in apertures of *ISO* and *Spitzer* observations. The *ISO*/SWS spectrum is more noisy than the IRS spectra, and the measurement of some weak features (e.g., [Mg V]) may not be reliable. The [S III] line in the *ISO* spectra is abnormally high which may be the result of contamination.

2.5. Spectral Energy Distribution

In order to ascertain the degree of contributions from the gas and dust components of NGC 6072, we have constructed

Figure 7. *Spitzer* IRS spectrum of NGC 6072.

a spectral energy distribution (SED) of using the IRAC and *IRAS* infrared photometry, as well as ground-based optical photometric measurements of the central star (Figure 8). The *IRAS* photometry measurements are taken from the *IRAS* Point Source Catalog whereas the IRAC photometric measurements are derived from summing the observed fluxes over the IRAC 4-band images and subtracting the respective background fluxes in the images. We can see that the *IRAS* photometry is entirely due to dust emission, whereas the IRAC photometry suggests a combination of nebular and dust emissions. After correcting the optical photometry by an extinction value of 1.32 (Shaw & Kaler 1989), the extinction-corrected emergent flux ($F_\lambda(\text{total})$) is then fitted by a three-component model (a hot central star, an ionized nebula, and a cool dust shell) using a procedure similar to that of Zhang & Kwok (1991):

$$F_\lambda(\text{total}) = F_\lambda(s) + F_\lambda(g) + F_\lambda(d), \quad (1)$$

where $F_\lambda(s)$, $F_\lambda(g)$, and $F_\lambda(d)$ are the flux densities of the photospheric continuum of the central star, the nebular continuum emission flux, and the dust thermal emission flux. Specifically

$$F_\lambda(s) = (\pi \theta_*^2) B_\lambda(T_*), \quad (2)$$

Table 3
The Parameters of the Two Ellipses

Ellipse	Center R.A. (J2000)	Center Decl. (J2000)	Major Axis	Minor Axis	Major Axis P.A.
1	16:12:58.306	-36:13:54.32	84''	26''	5°
2	16:12:58.534	-36:13:49.45	66''	20''	135°

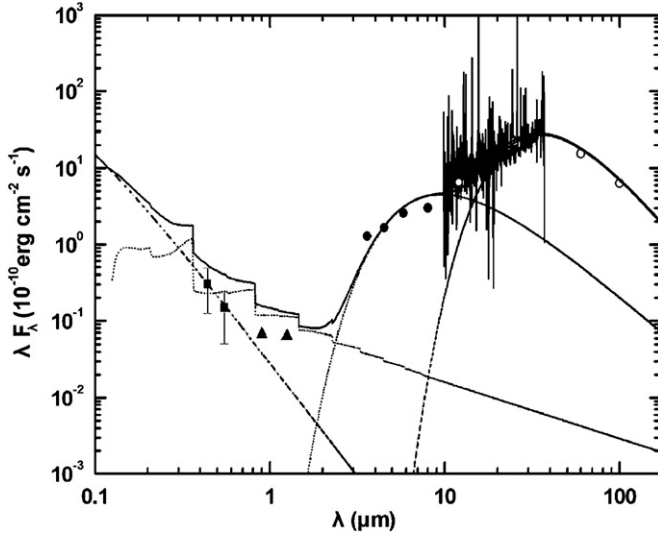


Figure 8. SED of NGC 6072. The open circles are *IRAS* 12, 25, 60, and 100 μm photometry, the filled-circles are the *IRAC* 4-band photometry, the triangles are *DENIS* near-IR photometry, the filled squares are *V* and *R* photometry of the central star. The dotted and long-dashed lines are blackbody fits to the dust continuum, the short-dashed line is a nebular $b-f+f-f$ emission model, and the dot-dashed line is a blackbody fit to the photospheric continuum of the central star. The total fluxes from all components are plotted as a solid line.

where θ_* and T_* are the angular radius and the effective temperature of central star, respectively, and $B_\lambda(T_*)$ is the Planck function for a temperature of T_* . In the model shown in Figure 8, we assume a central star temperature of 115,000 K and an extinction coefficient of 1.32. $F_\lambda(g)$ is the sum of the $b-f$, $f-f$ and two-photon emissions using the emission coefficients given in Kwok (2007) and assuming an electron temperature $T_e = 10^4$ K and an electron density $n_e = 10^3 \text{ cm}^{-3}$. Emission from the dust component is given by

$$F_\lambda(d) = \frac{M_d Q_\lambda B_\lambda(T_d)}{\frac{4}{3} a \rho_s D^2}, \quad (3)$$

where M_d is the dust mass, a is the grain radius, ρ_s is the grain density, $Q = Q_0(\lambda/\lambda_0)^{-\alpha}$ is the grain emissivity function, and D is the distance to the nebula (Kwok 2007, Equation (10.23)). We find that the dust emission component is too broad to be fit by a single dust temperature. Instead we assume that there are two dust components of temperatures 534 K and 105 K. Assuming $a = 0.1 \mu\text{m}$, $\rho_s = 1 \text{ g cm}^{-3}$, $\alpha = 1$, $Q(1 \mu\text{m}) = 0.1$, $D = 1 \text{ kpc}$, we derive dust masses of $1.0 \cdot 10^{-9} M_\odot$ and $1.1 \cdot 10^{-4} M_\odot$ for the warm and cold dust components, respectively. Assuming a typical dust-to-gas mass ratio of 3×10^{-3} , the dust mass implies that there is $\sim 0.04 M_\odot$ of gas mass in the dust component.

From the total observed nebular flux of $1.26 \times 10^{-10} \text{ erg cm}^{-2} \text{ s}^{-1}$, we derive an emission measure of $4.2 \times 10^{58} \text{ cm}^{-3}$. Assuming a distance of 1 kpc and an electron density of 10^3 cm^{-3} , we obtain a total ionized gas mass of $0.13 M_\odot$. In comparison, the molecular mass as derived from CO observations is $0.22 M_\odot$ (Cox et al. 1991).

The above model fits suggest that the fraction of fluxes emerging from the stellar, nebular, and dust components are 64%, 7%, and 29%, respectively, and the total amount of mass in the PN is larger than that of the ionized mass seen in the optical image. Where does this invisible mass lie? This question can only be answered observationally by mid-infrared or submillimeter molecular imaging. However, assuming that the ring seen in the *Spitzer* and *CFHT* images is an equatorial disk, then the lobes must be confined by an external medium around the equatorial (N-S) directions. A significant fraction of the unseen mass is likely to be located in this region.

3. MODEL OF A DOUBLE-BIPOLAR LOBE SYSTEM

NGC 6072 shares some common structural similarities with other multipolar PNs. He 2-47 has three pairs of bipolar lobes and a central equatorial region. The equatorial region actually consists of two partial rings (Sahai 2000, Figure 1(b)). One is therefore tempted to assume that each pair of the bipolar lobes may be associated with one equatorial torus. We would like to explore further what the appearances of such multiple systems may look like when viewed from different perspectives.

We have constructed a schematic model of a double bipolar system using the *SHAPE* software (Steffen & López 2006). The object NGC 6072 is used as a guide, but the model is not meant to be a model fit of the object. We first rotate the image of NGC 6072 such that the major axis of ring d is along the vertical direction (Figure 9), which corresponds to a P.A. = 5° in Figure 2. In order to highlight the main structures, the contrast in Figure 9 is adjusted to show only the brightest parts of NGC 6072. If the bright eastern part of the northern “bar” discussed in section 2.2 is part of the equatorial ring, one might assume that the western part of this “bar” is part of a second ellipse. A sketch of these two ellipses is shown in Figure 9 and their parameters are listed in Table 3. The center of ring 2 is shifted by 5'' from that of ring 1, along P.A. = 5° (J2000). It turns out that these two rings have similar major-to-minor axis ratios. If we interpret the two ellipses as two tilted circular rings, then the observed major-to-minor axis ratio implies a tilting angle of the rings of 72° from the plane of sky. Since it is hard to tell which side is tilting toward us, we just arbitrarily choose the east side of ring 1 and the NE side of ring 2 to be the blueshifted sides.

We further created two pairs of lobes with their symmetry axes perpendicular to the two rings, and with their respective centers coinciding with the centers of the two rings. Therefore the nebula is modeled as two bipolar systems, each consisting of a pair of bipolar lobes and an equatorial ring. The length of the lobes in systems 1 and 2 are 96'' and 75'', after the effects of tilting have been corrected. The symmetry axes of the two systems are along P.A. = 95° and 45°. Since the axes are tilted by 72° with the line of sight, in three dimensional the two axes are actually separated by 47°. The shape of the two systems is similar and just differ in size by a multiplication factor of 1.27 for both the ring and the lobes. This number could imply the different time at which the two systems were formed. The corresponding dynamical times of the two systems are 18,000 and 14,000 (D/kpc) ($V/25 \text{ km s}^{-1}$)⁻¹ yr, respectively.

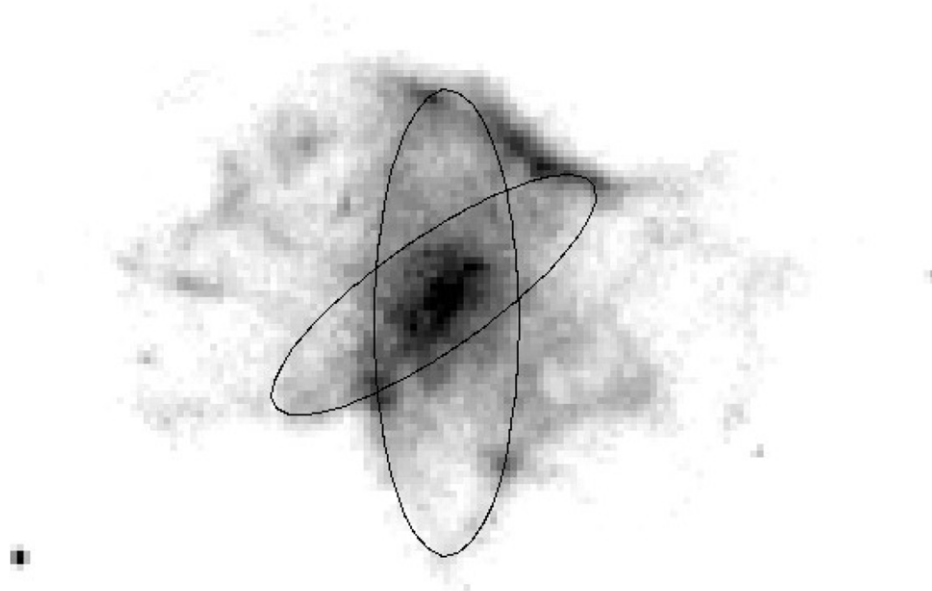


Figure 9. Brighter part of the $8 \mu\text{m}$ IRAC image of NGC 6072 with the schematic drawing of the two rings superimposed.

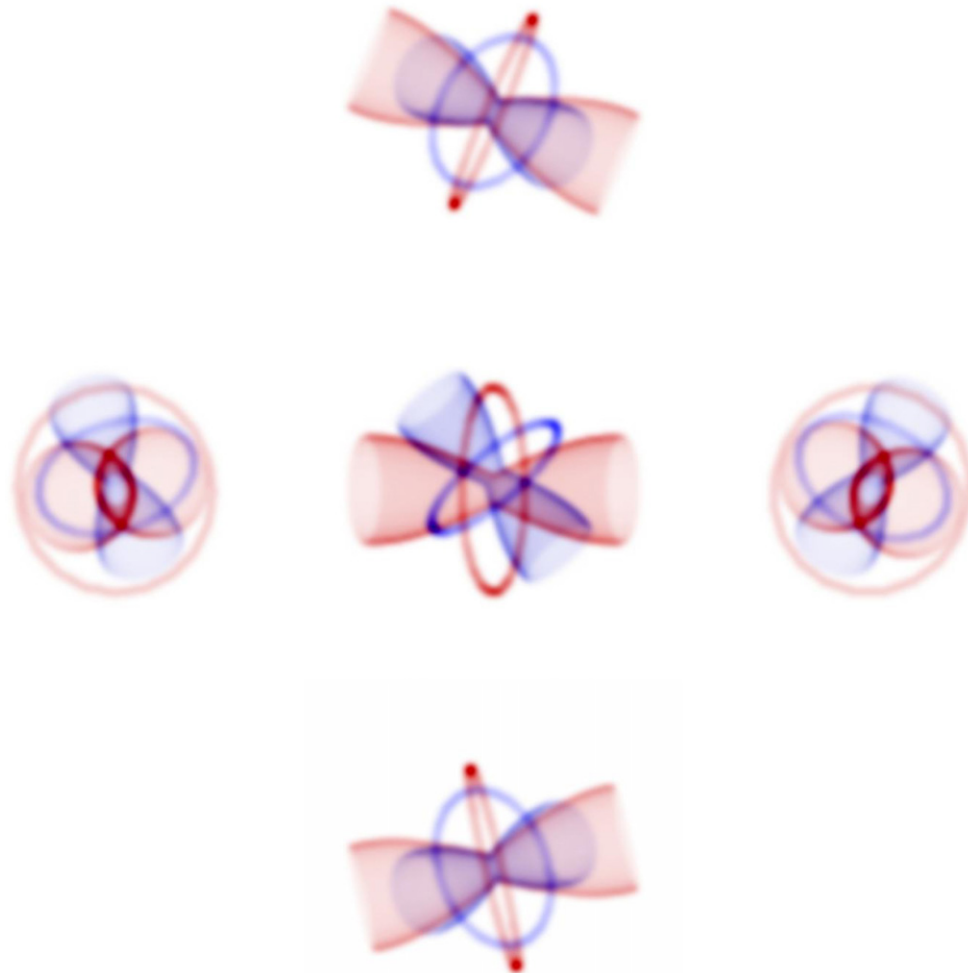


Figure 10. Model viewed at different angles. System 1 is in red, while system 2 is in blue. The central image is as seen from Earth, while the other four, starting from above and in a clockwise sense, are views from the top, right, bottom, and left, respectively.

(A color version of this figure is available in the online journal.)

The model is not meant to account for all the features seen in the observed images of NGC 6072, but to provide an illustration of the complexity of the system. In Figure 10, we show the

model nebula being viewed from different perspectives. In the top and bottom views, the equatorial ring of system 1 is viewed edge on, and the nebula has a clearly bipolar structure with

an inner and outer lobes, as in NGC 6884. In the right and left views, the equatorial ring of system 1 appears circular, and when viewed alone, may be taken as the projection of a spherical shell. Had our line of sight to NGC 6072 been along any of these directions, it would be very difficult to realize that NGC 6072 is a multipolar system.

4. DISCUSSIONS

For most of the 200 years since the discovery of the first PNs, astronomers have always assumed that PNs are a shell of ionized gas radiating mostly in atomic lines. The existence of bipolar nebulae such as NGC 2346 and NGC 6302 raises the question on the origin of these morphologies. Higher dynamic-range observations reveal, however, that even objects with apparent elliptical structures can actually be bipolar nebulae. Some examples are NGC 650-1, Sh 1-89, and SaWe 3 (Hua 1997; Hua et al. 1998). PNs with well-defined ring-like structures such as NGC 7027 and NGC 3132 are in fact bipolar nebulae, with the bright ring corresponding to the torus of the bipolar nebulae (Latter et al. 2000; Monteiro et al. 2000). Even well-known objects such as NGC 6720 (the Ring Nebula) and NGC 7293 (the Helix Nebula) are believed to be bipolar (Bryce et al. 1994; Meaburn et al. 2005). The population of bipolar PNs therefore is much larger than what it appears to be.

Some prominent bipolar PNs on closer inspection are actually multipolar objects. Some examples are NGC 2440 (López et al. 1998) and NGC 6881 (Kwok & Su 2005). Mampaso et al. (2006) have found a new PN with an equatorial ring, a pair of inner lobes, a pair of bright main lobes, and very large faint outer lobes. The symmetry axes of these lobes all seem to have different orientations. Our present observations show that NGC 6072 certainly is not adequately described by the traditional round, elliptical, and butterfly schemes, and has a much more complicated morphological structure with multiple symmetry axes.

There are other examples of PNs with multiple rings and lobes. The apparent structure of NGC 6072 bears some resemblance to NGC 7026. At least two pairs of bipolar lobes are clearly visible beyond the central elliptical ring in the *Hubble Space Telescope* image of this object (Kwok 2001). Kinematic studies have also suggested NGC 7026 to be a multipolar nebula (Cuesta et al. 1995; López 2002). Also interesting to compare is IRAS 19024+0044, a proto-PN with three pairs of bipolar lobes and possibly two equatorial tori (Sahai et al. 2005b). The compact PN He 2–47 has two partial rings that are coplanar, but He 2–113 have two non-coplanar rings that are not orthogonal to the bipolar axes (Sahai 2000; Sahai et al. 2005a, 2005b). With such a variety of rings and lobes, it is difficult to make any definitive conclusions on the cause–effect relationship between these structures.

Since most PNs have not been observed with the angular resolution and dynamic range necessary to detect the multipolar lobes, the number of known cases for multipolar nebulae may be regarded as only the tips of icebergs. Further deep and wide-field imaging of PNs will lead to a greater appreciation of the complexity of the PN morphology. Ultimately the confirmation of the multipolar structure has to come from kinematic studies and integral field spectroscopy of PNs will have a significant impact in this regard.

5. CONCLUSIONS

From near-infrared imaging of the PN NGC 6072, we have found a clear elliptical ring in the system, which we interpret

to be the result of an equatorial outflow. Also seen are three pairs of bipolar lobes, indicating that NGC 6072 is a multipolar system. The case of NGC 6072 further suggests that multipolar nebulae may be a common phenomenon and more examples may emerge as deeper imaging is done for a larger sample of PNs. While the morphology of PNs is the result of the dynamical interaction between collimated fast outflows with the remnants of previously ejected materials, the existence of multipolar PNs suggests that the fast outflows may have suffered from a changing of orientation with time. The physical cause of such changes represents an interesting unsolved problem of PN dynamics.

This work is based in part on observations made with the *Spitzer Space Telescope*, which is operated by the Jet Propulsion Laboratory, California Institute of Technology under a contract with NASA, and in part based on observations obtained at the CFHT which is operated by the National Research Council of Canada, the Institut National des Sciences de l'Univers of the Centre National de la Recherche Scientifique of France, and the University of Hawaii. Access to the CFHT was made possible by the Ministry of Education and the National Science Council of Taiwan as part of the Cosmology and Particle Astrophysics (CosPA) initiative. The work was supported by a grant from the Research Grants Council of the Hong Kong Special Administrative Region, China (project no. HKU 7028/07P). N.K. acknowledges support by the Natural Sciences and Engineering Council of Canada, Alberta Ingenuity, and the Killam Trusts.

REFERENCES

- Acker, A., Ochsenbein, F., Stenholm, B., Tylenda, R., Marcout, J., & Schohn, C. 1992, *Strasbourg-ESO Catalogue of Galactic Planetary Nebulae* (Garching: ESO)
- Bryce, M., Balick, B., & Meaburn, J. 1994, *MNRAS*, **266**, 721
- Corradi, R. L. M., & Schwarz, H. E. 1995, *A&A*, **293**, 871
- Cox, P., Huggins, P. J., Bachiller, R., & Forveille, T. 1991, *A&A*, **250**, 533
- Cuesta, L., Phillips, J. P., & Mampaso, A. 1995, in *Ann. Israel Phys. Soc.* 11, *Asymmetrical Planetary Nebulae*, ed. A. Harpaz & N. Soker (Bristol: IOP Publishing), 158
- Gathier, R., & Pottasch, S. R. 1988, *A&A*, **197**, 266
- Higdon, S. J. U., et al. 2004, *PASP*, **116**, 975
- Houck, J. R., et al. 2004, *ApJS*, **154**, 18
- Hua, C. T. 1997, *A&AS*, **125**, 355
- Hua, C. T., Dopita, M. A., & Martinis, J. 1998, *A&AS*, **133**, 361
- Hubble, E. 1921, *PASP*, **33**, 175
- Huggins, P. J., & Healy, A. P. 1989, *ApJ*, **346**, 201
- Kwok, S. 2001, *Cosmic Butterflies* (Cambridge: Cambridge Univ. press), 78
- Kwok, S. 2007, *Physics and Chemistry of the Interstellar Medium* (Sausalito, CA: Univ. Science Books)
- Kwok, S., & Su, K. Y. L. 2005, *ApJ*, **635**, L52
- Latter, W. B., Dayal, A., Bieging, J. H., Meakin, C., Hora, J. L., Kelly, D. M., & Tielens, A. G. G. M. 2000, *ApJ*, **539**, 783
- Liu, X.-W., et al. 2001, *MNRAS*, **323**, 343
- López, J. A. 2002, *RevMexAA*, **13**, 139
- López, J. A., Meaburn, J., Bryce, M., & Holloway, A. J. 1998, *ApJ*, **493**, 803
- Mampaso, A., et al. 2006, *A&A*, **458**, 203
- Manchado, A., Stanghellini, L., & Guerrero, M. A. 1996, *ApJ*, **466**, L95
- Meaburn, J., Boumis, P., López, J. A., Harman, D. J., Bryce, M., Redman, M. P., & Mavromatakis, F. 2005, *MNRAS*, **360**, 963
- Monteiro, H., Morisset, C., Gruenwald, R., & Viegas, S. M. 2000, *ApJ*, **537**, 853
- Sahai, R. 2000, *ApJ*, **537**, L43
- Sahai, R., Nyman, L.-Å., & Wootten, A. 2005, *ApJ*, **543**, 880
- Sahai, R., Sánchez Contreras, C., & Morris, M. 2005, *ApJ*, **620**, 948
- Shaw, R. A., & Kaler, J. B. 1989, *ApJS*, **69**, 495
- Steffen, W., & López, J. A. 2006, *RevMexAA*, **42**, 99
- Zhang, C. Y., & Kwok, S. 1991, *A&A*, **250**, 179